ELSEVIER

Materials Chemistry and Physics 72 (2001) 281–285

MATERIALS CHEMISTRY AND PHYSICS

www.elsevier.com/locate/matchemphys

Chemical control of colossal magnetoresistance in manganites

Chih-Hung Shen [a], Ru-Shi Liu [a,*], Ravi Gundakaram [a], Shu-Fen Hu [b], Jauyn Grace Lin [c], Chao-Yuan Huang [c,d,e], Chien-Min Wang [f]

[a] *Department of Chemistry, National Taiwan University, No. 1 Roosevelt Road, Section 4, Taipei 106, Taiwan*
[b] *National Nano Device Laboratories, Hsinchu, Taiwan*
[c] *Center for Condensed Matter Sciences, National Taiwan University, Taipei, Taiwan*
[d] *Department of Physics, National Taiwan University, Taipei, Taiwan*
[e] *Department of Electrical Engineering, National Taiwan University, Taipei, Taiwan*
[f] *SYNergy ScienTech Corp., Hsinchu, Taiwan*

Abstract

The evolution of the structural, electrical and magnetic properties with the isovalent chemical substitution of Ca^{2+} into the Sr^{2+} sites in the new series of two-dimensional $La_{1.2}(Sr_{1.8-x}Ca_x)Mn_2O_7$ samples ($0 \leq x \leq 0.8$) and three-dimensional $La_{0.6}(Sr_{0.4-x}Ca_x)MnO_3$ samples ($0 \leq x \leq 0.4$) has been investigated. The compositional dependence of the structural variation has been found in $La_{0.6}(Sr_{0.4-x}Ca_x)MnO_3$. The Curie temperatures (T_C) decreased from 135 to 102 K and 370 to 270 K for $x = 0$–0.4 in $La_{1.2}(Sr_{1.8-x}Ca_x)Mn_2O_7$ and $La_{0.6}(Sr_{0.4-x}Ca_x)MnO_3$, respectively. Our results confirm that the dimensionality as well as ionic size plays an important role in controlling the colossal magnetoresistance in manganites. © 2001 Elsevier Science B.V. All rights reserved.

Keywords: Magnetic structure; XRD; TEM; Magnetometer

1. Introduction

Since the discovery of high-temperature superconductivity in perovskite copper oxides, there has been revived interest in mixed valence transition metal oxides. The ABO_3-type manganites $R_{n+1}Mn_nO_{3n+1}$ (R = rare earth and $n = \infty$), exhibit colossal magnetoresistance (CMR) in a relatively small temperature range around the Curie temperature (T_C) [1]. CMR is the large decrease in resistance under an applied magnetic field, concomitant with a paramagnetic insulator-like phase at high temperature and a ferromagnetic metallic phase at low temperature. Suitable substitution of A^{2+} ions for R^{3+} ions results in Mn^{3+}/Mn^{4+} mixed valence, and hence the strong coupling between the magnetic ordering and the electrical conductivity leading to a strong relationship between the electrical resistivity and the spin alignment, which has been explained by the double-exchange mechanism [2]. This mechanism describes the transfer of an electron between the Mn^{3+} and Mn^{4+} ions. The electrons in the e_g orbitals of Mn^{3+} ($t_{2g}{}^3e_g{}^1$) ions are the charge carriers that move in a background of Mn^{4+} ($t_{2g}{}^3$) ions. The alignment of the Mn^{4+} localized spins favors the delocalization of the e_g electrons and reduces the total energy of the system.

In the Ruddlesden–Popper (RP) $La_{n-nx}(Sr, Ca)_{1+nx}Mn_nO_{3n+1}$ system, the dimensionality can be varied by increasing the number of perovskite layers and by controlling the arrangement of MnO_6 octahedra. Many interesting studies have been carried out on the manganites of the series $La_{n-nx}Sr_{1+nx}Mn_nO_{3n+1}$ with $x = 0.4$ and $n = 2$. $La_{1.2}Sr_{1.8}Mn_2O_7$ is a conducting ferromagnet with a T_C of 130 K and with a high MR value; this composition is a paramagnetic insulator above T_C [3,4]. The $c = 2$ member of the RP series exhibits conducting ferromagnetic behavior with a MR ratio ($[\rho(0) - \rho(H)/\rho(0)]$) higher than that of the $n = 3$ and ∞ members, where $\rho(0)$ is the resistivity in zero field and $\rho(H)$ is the resistivity under a field of 1.5 T [1]. This implies that a lower dimensionality is more favorable for CMR. However, the properties of the solid solution of Sr^{2+} and Ca^{2+} in $La_{1.2}(Sr_{1.8-x}Ca_x)Mn_2O_7$ have not been systematically studied.

In the $n = \infty$ compounds, the gradual replacement of Ca^{2+} by Sr^{2+} in $La_{0.75}(Ca_{0.25-x}Sr_x)MnO_3$ results in an increase of T_C from ~225 K ($x = 0$) to ~340 K ($x = 0.25$) [5]. The phase transformation from orthorhombic to rhombohedral has been observed in the $La_{0.75}(Ca_{0.25-x}Sr_x)MnO_3$ system with fixed Mn valence, which is difficult to explain as the effect of increasing the Mn valence. There-

* Corresponding author. Tel.: +886-2-2369-0152; fax: +886-2-2363-6359.
E-mail address: rsliu@ccms.ntu.edu.tw (R.-S. Liu).

0254-0584/01/$ – see front matter
PII: S0254-0584(01)00453-9

fore, a detailed study on the phase transformation is very informative.

In this paper, we report the evolution of the structural, electrical and magnetic properties of $La_{1.2}(Sr_{1.8-x}Ca_x)Mn_2O_7$ ($0 \leq x \leq 0.8$) possessing the layered structure, and $La_{0.6}(Sr_{0.4-x}Ca_x)MnO_3$ ($0 \leq x \leq 0.4$) with the 3D structure, wherein isovalent chemical substitution of Ca into the Sr sites has been carried out.

2. Experimental

High purity powders of La_2O_3, $SrCO_3$, $CaCO_3$ and MnO_2 were weighed in appropriate proportions to obtain the nominal compositions of $La_{1.2}(Sr_{1.8-x}Ca_x)Mn_2O_7$ ($0 \leq x \leq 0.8$) [6] and $La_{0.6}(Sr_{0.4-x}Ca_x)MnO_3$ ($0 \leq x \leq 0.4$). The former were calcined in air for 24 h at 1200°C and the latter for 24 h at 900°C. Then, the samples were sintered in air at 1400–1500°C for 72 h with an intermediate grinding after every 24 h. X-ray powder diffraction (XRD) measurements were carried out with a SCINTAG (X1) diffractometer (Cu Kα radiation, $\lambda = 1.5406$ Å) at 40 kV and 30 mA. The program GSAS [7] was used for the Rietveld refinement in order to obtain the structural parameters. High-resolution transmission electron microscopy (HRTEM) was carried out using a JEOL 4000EX electron microscope operating at 400 kV. Magnetization data were collected on a superconducting quantum interference device (SQUID) magnetometer (quantum design).

3. Results and discussion

In Fig. 1, we show the XRD patterns of the series $La_{1.2}(Sr_{1.8-x}Ca_x)Mn_2O_7$ ($0 \leq x \leq 0.8$). All of the samples are of single phase. The samples can be indexed to the $Sr_3Ti_2O_7$-type structure with a tetragonal unit cell (space group: *I4/mmm*). Based on our XRD refinements, both lattice constants (*a* and *c*) and cell volume (*V*) decrease as the Ca content increases. The structural changes are simply due to a manifestation of the size effect between Ca^{2+} (1.18 Å for CN (coordination number) = 9) and Sr^{2+} (1.31 Å for CN = 9) [4]. The bottom left portion of Fig. 2 shows the crystal structure of $La_{1.2}(Sr_{1.4}Ca_{0.4})Mn_2O_7$ which consists of double perovskite layers, each layer consisting of a two-dimensional network of MnO_6 octahedra. The unit cell is shown with a solid line and the arrangement of MnO_6 octahedra is shaded. This model is also supported by HRTEM observations. Fig. 2 shows the HRTEM image with the incident electron beam along the [1 1 0] direction. The corresponding selected area electron diffraction pattern is shown in the top left. The lattice image clearly shows layers with uniform spacing of about 10 Å, which corresponds to nearly half the *c*-axis unit length. There are no stacking faults as can be observed from this image, indicating a high homogeneity in this compound. The electron diffraction pattern can be indexed with respect to the $h + k + l = 2n$ reciprocal lattice sections of the tetragonal cell with $a = b \sim 3.9$ Å and $c \sim 20$ Å.

The powder XRD patterns of the $La_{0.6}(Sr_{0.4-x}Ca_x)MnO_3$ ($0 \leq x \leq 0.4$) samples are shown in Fig. 3(a). All the samples of this series are of single phase. For the samples with $x = 0$ and 0.4, all the peaks in each pattern can be indexed with a rhombohedral unit cell (space group: *R*-3*c*) and orthorhombic (space group: *Pbnm*), respectively. As *x* increases to 0.3, some reflections merge together, which indicates that in the region $x < 0.3$, the structure is rhombohedral and for $x \geq 0.3$, the structure becomes orthorhombic. An increase in the Ca content in $La_{0.6}(Sr_{0.4-x}Ca_x)MnO_3$ leads to an increase in the distortion of the MnO_6 octa-

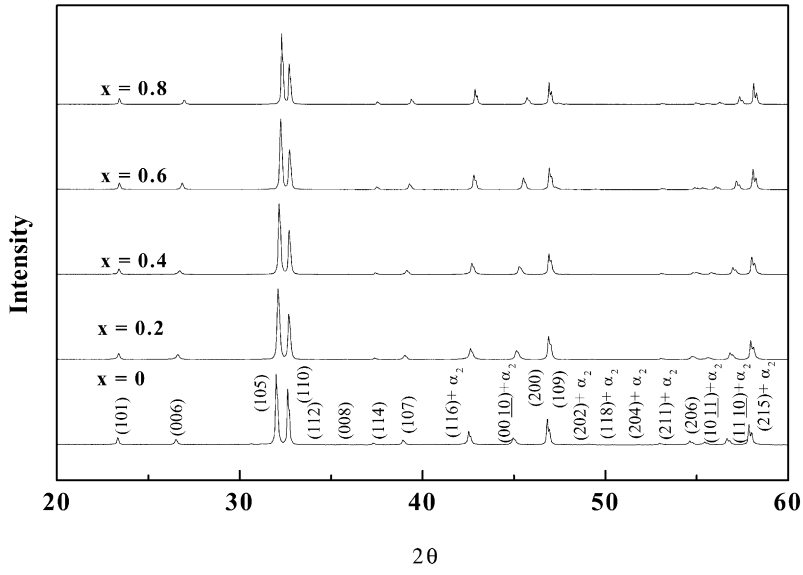

Fig. 1. Powder XRD patterns of the $La_{1.2}(Sr_{1.8-x}Ca_x)Mn_2O_7$ samples.

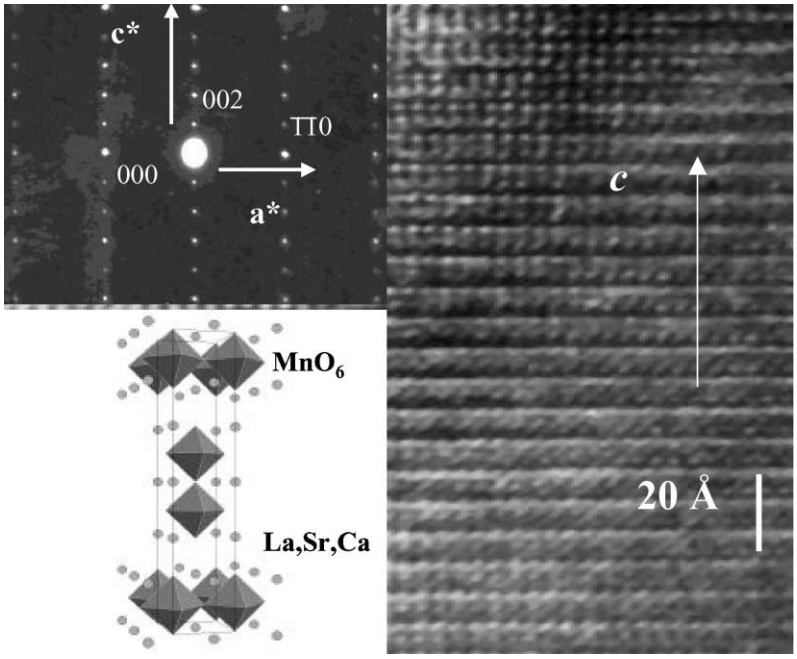

Fig. 2. HRTEM image along the *c*-axis for $La_{1.2}(Sr_{1.4}Ca_{0.4})Mn_2O_7$. The top left portion shows the electron diffraction pattern along [1 1 0] of the tetragonal cell.

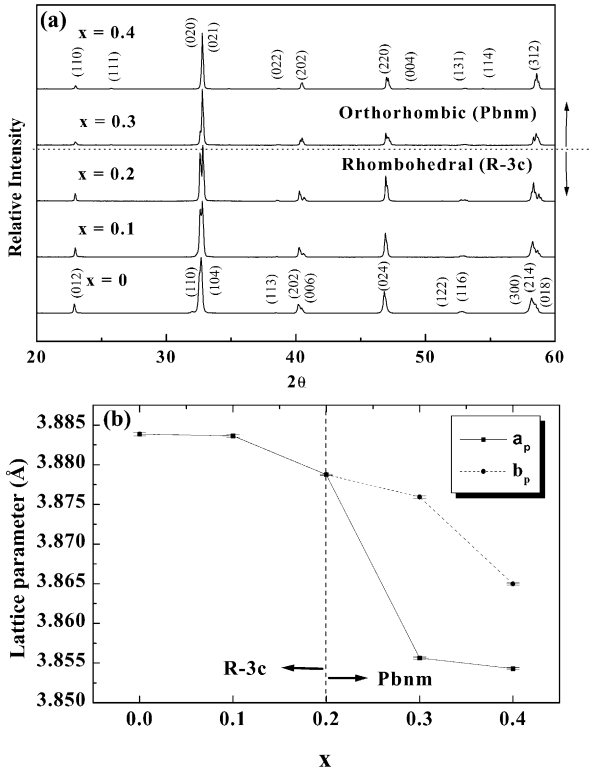

Fig. 3. (a) XRD patterns of the series $La_{0.6}(Sr_{0.4-x}Ca_x)MnO_3$. (b) Basic perovskite cell parameters (a_p and b_p) as a function of x in $La_{0.6}(Sr_{0.4-x}Ca_x)MnO_3$.

hedra. The basic perovskite lattice constants (a_p and b_p) also decrease as x increases (as shown in Fig. 3(b)).

The crystal structure and the results of HRTEM of $La_{0.6}(Sr_{0.4-x}Ca_x)MnO_3$ are shown in Fig. 4. The HRTEM lattice image along [1 1 1] zone-axis direction of $La_{0.6}(Sr_{0.4-x}Ca_x)MnO_3$ ($x = 0.1$) is shown in Fig. 4(a). The inset of Fig. 4(a) shows the structural model along [1 1 1] of the rhombohedral cell (space group: *R-3c*) of $La_{0.6}(Sr_{0.4-x}Ca_x)MnO_3$. The corresponding lattice image is in agreement with the model. Fig. 4(b) shows the HRTEM lattice image along the [0 1 0] zone-axis direction of $La_{0.6}(Sr_{0.4-x}Ca_x)MnO_3$ ($x = 0.3$). The structural model along [0 1 0] of the orthorhombic cell (space group: *Pbnm*) is shown in the inset of Fig. 4(b). The perfect order along the *c*-axis is confirmed by the HRTEM image. No superstructures were found in the $La_{0.6}(Sr_{0.4-x}Ca_x)MnO_3$ ($0 \leq x \leq 0.4$) series samples.

The temperature dependence of the magnetization in an applied field of 0.1 T for $La_{1.2}(Sr_{1.8-x}Ca_x)Mn_2O_7$ ($0 \leq x \leq 0.8$) and $La_{0.6}(Sr_{0.4-x}Ca_x)MnO_3$ ($0 \leq x \leq 0.4$) is shown in Fig. 5(a) and (b), respectively. A systematic analysis of the phase diagram of the transition temperature (T_C) versus the concentration of Ca^{2+} for $La_{1.2}(Sr_{1.8-x}Ca_x)Mn_2O_7$ indicates that the T_C decreases from 135 to 71 K for $x = 0$–0.8. For the series $La_{0.6}(Sr_{0.4-x}Ca_x)MnO_3$, paramagnetic to ferromagnetic transitions are observed in the temperature range of 250–350 K, as can be seen from Fig. 5(b). A decrease in the T_C's from a value greater than 350 K for $x = 0$ to 270 K for $x = 0.4$ has been observed. These results lead to the understanding that the T_C is very sensitive

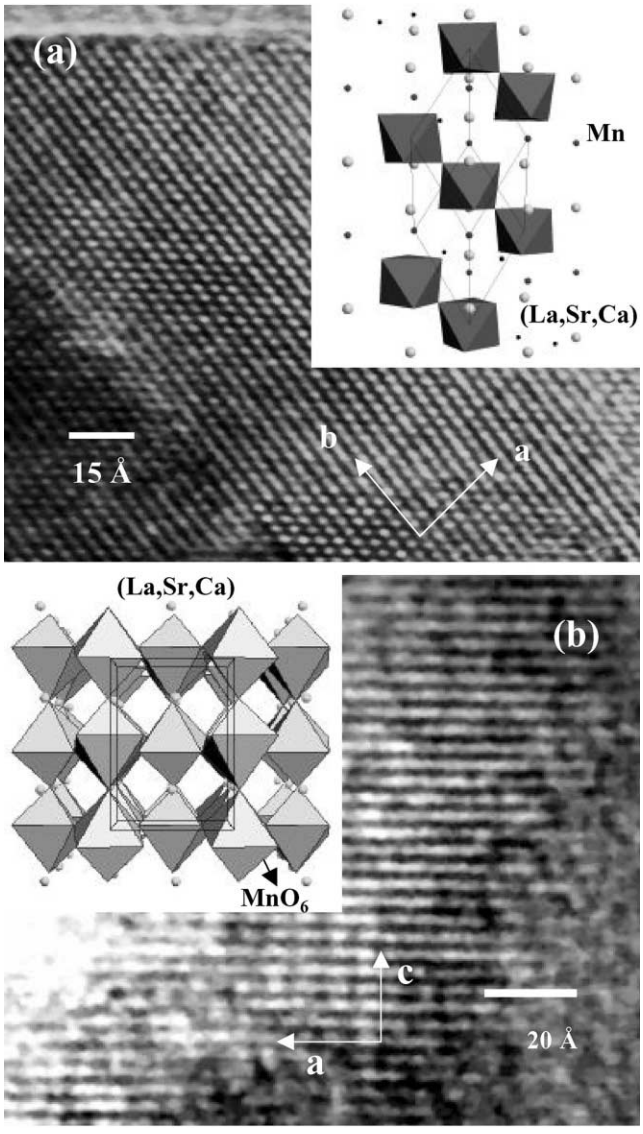

Fig. 4. HRTEM lattice images taken along the (a) [0 0 1] zone-axis directions of the $La_{0.6}(Sr_{0.4-x}Ca_x)MnO_3$ sample with $x = 0.1$. The corresponding rhombohedral structure is shown in the inset of (a). (b) [0 1 0] zone-axis directions of the $La_{0.6}(Sr_{0.4-x}Ca_x)MnO_3$ sample with $x = 0.3$. The corresponding orthorhombic is shown in the inset of (b).

to chemical pressure (i.e., structural distortions induced by changing the average radius of the cations). This suggests that the smaller Ca^{2+} ions substituting into the bigger Sr^{2+} sites leads to a decrease in T_C. Based on the model of double exchange, a lower T_C corresponds to a poor overlap between Mn 3d and O2p orbitals resulting in a reduced bandwidth (W) [8,9]. With increasing Ca content, there is a decrease in the overlap between Mn $3d_z{}^2$ and $O2p_z$ which may result in a decrease in T_C's. Therefore, the structural transformation of the $La_{0.6}(Sr_{0.4-x}Ca_x)MnO_3$ compositions from rhombohedral to orthorhombic by chemical substitution of isovalent Ca^{2+} for Sr^{2+} causes a decrease in

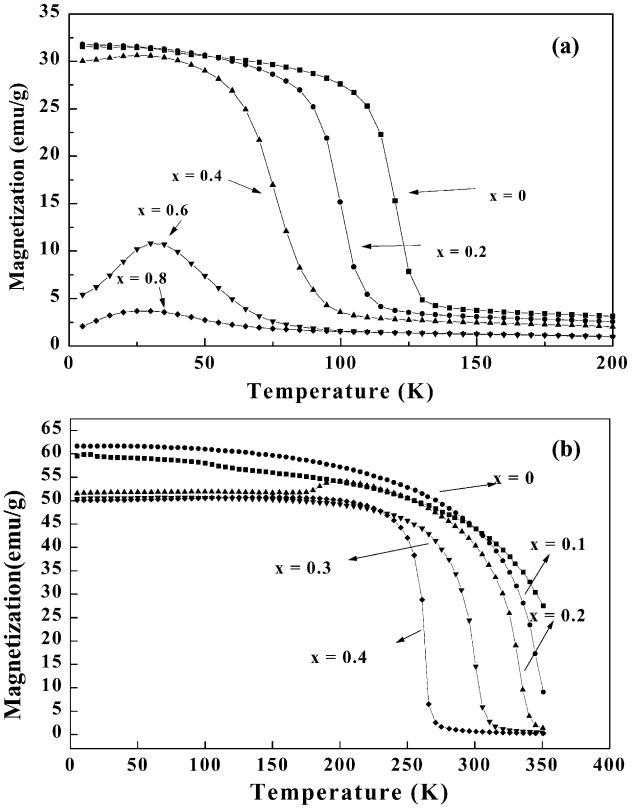

Fig. 5. Temperature dependence of magnetization at a magnetic field of 0.1 T for the series: (a) $La_{1.2}(Sr_{1.8-x}Ca_x)Mn_2O_7$ ($x = 0$–0.8); (b) $La_{0.6}(Sr_{0.4-x}Ca_x)MnO_3$ ($x = 0$–0.4).

T_C due to poor hybridization between Mn $3d_z{}^2$ and $O2p_z$ in the orthorhombic cell. The results are consistent with the series $La_{0.6}(Sr_{0.4-x}Ca_x)MnO_3$ with $x \geq 0.3$ exhibiting a distorted MnO_6 octahedral structure which indicates that the Jahn–Teller distortion occurs along the c-axis in these

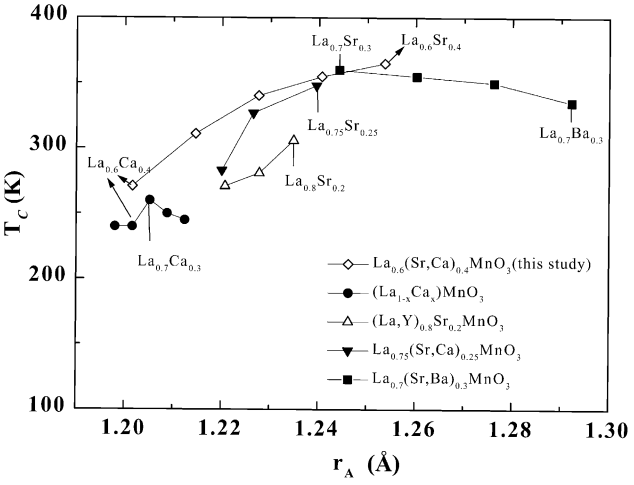

Fig. 6. Variation of T_C of (Ln, A)MnO_3 as a function of the average radius $\langle r_A \rangle$ of the Ln/A (Ln = La or Y; A = Ca, Sr or Ba) cations.

compounds. Such an effect would lead to a decrease in the spatial overlap of the Mn $3d_z{}^2$ and $O2p_z$ orbital.

In Fig. 6, we show the T_C's of (Ln, A)MnO_3 as a function of the average radius (assuming ninefold coordination) of the Ln/A (Ln = La or Y; A = Ca, Sr or Ba) cations, $\langle r_A \rangle = [(1-x)r_{Ln} + xr_A]$. The data in this figure include results from our study on the series $La_{0.6}(Sr_{0.4-x}Ca_x)MnO_3$, as also those from earlier studies [5,9,10]. An increase in $\langle r_A \rangle$ gives rise to an increase in T_C. Therefore, the isovalent chemical substitution of the smaller Ca^{2+} ions into the bigger Sr^{2+} sites in the series $La_{n-nx}(Sr, Ca)_{1+nx}Mn_nO_{3n+1}$ causes the decrease of the T_C's.

4. Conclusion

In conclusion, an investigation of the new series of two-dimensional $La_{1.2}(Sr_{1.8-x}Ca_x)Mn_2O_7$ ($0 \leq x \leq 0.8$) and three-dimensional $La_{0.6}(Sr_{0.4-x}Ca_x)MnO_3$ ($0 \leq x \leq 0.4$) manganites has allowed us to establish the relationship between the ionic size and T_C. This study has demonstrated that the size of the interpolated cation by tuning the concentration between Ca^{2+} and Sr^{2+} plays a crucial role in controlling the magnetotransport properties in the $La_{n-nx}(Sr, Ca)_{1+nx}Mn_nO_{3n+1}$ compositions.

Acknowledgements

The work is supported by the National Science Council of the ROC under the grant numbers of NSC 89-2113-M-002-004 and NSC 89-2112-M-002-030.

References

[1] R. Mahesh, R. Mahendiran, A.K. Raychaudhuri, C.N.R. Rao, J. Solid State Chem. 122 (1996) 448.
[2] C. Zener, Phys. Rev. 82 (1951) 403.
[3] D.N. Argyriou, J.F. Mitchell, J.B. Goodenough, O. Chmaissem, S. Short, J.D. Jorgensen, Phys. Rev. Lett. 78 (1997) 1568.
[4] P.D. Battle, M.A. Green, N.S. Laskey, N. Jasmir, J.E. Millburn, L.E. Spring, S.P. Sullivan, M.J. Rosseinsky, J.F. Vente, J. Mater. Chem. 7 (1997) 977.
[5] Z.B. Guo, W. Yang, Y.T. Shen, Y.W. Du, Solid State Commun. 105 (1998) 89.
[6] C.-H. Shen, R.-S. Liu, S.-F. Hu, J.G. Lin, C.-Y. Huang, H.S. Sheu, J. Appl. Phys. 86 (1999) 2178.
[7] A.C. Larson, R.B. von Dreele, Generalized Structure Analysis System, Los Alamos National Laboratory, Los Alamos, NM, 1994.
[8] J.L. Garcia-Munoz, J. Fontcuberta, M. Suaaidi, X. Obradors, J. Phys. Condens. Matter 8 (1996) L787.
[9] P.G. Radaelli, G. Iannone, M. Marezio, H.Y. Huang, S.-W. Cheong, J.D. Jorgensen, D.N. Argyriou, Phys. Rev. B 56 (1997) 8265.
[10] H.Y. Hwang, S.-W. Cheong, P.G. Radaelli, M. Marezio, B. Batlogg, Phys. Rev. Lett. 75 (1995) 914.